Different shades of default mode disturbance in schizophrenia: Subnodal covariance estimation in structure and function

Jeremy Lefort-Besnard, Danielle S Bassett, Jonathan Smallwood, Daniel S. Margulies, Birgit Derntl, Oliver Gruber, Andre Aleman, Renaud Jardri, Gaël Varoquaux, Bertrand Thirion, et al.

HUMAN BRAIN MAPPING

Different shades of default mode disturbance in schizophrenia: Subnodal covariance estimation in structure and function

Journal:	*Human Brain Mapping*
Manuscript ID	HBM-17-1058.R1
Wiley - Manuscript type:	Research Article
Date Submitted by the Author:	20-Oct-2017
Complete List of Authors:	Lefort-Besnard, Jeremy; Rheinisch Westfalische Technische Hochschule Aachen, Department of Psychiatry, Psychotherapy, and Psychosomatics Bassett, Danielle; University of Pennsylvania, Bioengineering Smallwood, Jonathan; Max Plank Institute for Human Cognitive and Brain Sciences, Department of Social Neuroscience Margulies, Daniel; Max Planck Institute for Human Cognitive and Brain Sciences, Derntl, Birgit; Clinic for Psychiatry and Psychotherapy Tübingen Gruber, Oliver; Heidelberg University Hospital, General Psychiatry; Universitatsklinikum Gottingen, Center for Translational Research in Systems Neuroscience and Psychiatry, Department of Psychiatry and Psychotherapy Aleman, Andre; BCN Neuroimaging Center, University Medical Center Groningen, University of Groningen, Groningen, Netherlands Jardri, Renaud; Univ Lille, CNRS UMR9193, SCALab & CHU Lille, Fontan Hospital, CURE platform, 59000 Lille, France Varoquaux, Gael; INRIA, ; CEA, NeuroSpin Thirion, Bertrand; CEA, SHFJ Eickhoff, Simon; Research Center Jülich, Institut for Medicine (IME) Bzdok, Danilo; Heinrich Heine University, Institute of Clinical Neuroscience and Medical Psychology; Research Centre Jülich, Institute of Neuroscience and Medicine (INM-1)
Keywords:	Schizophrenia, Default mode network, Neuroimaging, Structural covariance, Functional connectivity, Sparse inverse covariance estimation, Machine learning

Different shades of default mode disturbance in schizophrenia: Subnodal covariance estimation in structure and function

Jérémy Lefort-Besnard[1], Danielle S. Bassett[2,9], Jonathan Smallwood[3], Daniel S. Margulies[4], Birgit Derntl[1,8,10], Oliver Gruber[11], Andre Aleman[12], Renaud Jardri[13], Gaël Varoquaux[5], Bertrand Thirion[5], Simon B. Eickhoff[6,7], Danilo Bzdok[1,5,8,*]

[1] Department of Psychiatry, Psychotherapy, and Psychosomatics, RWTH Aachen University, Germany
[2] Department of Bioengineering, University of Pennsylvania, Philadelphia, PA 19104, USA
[3] Department of Psychology, University of York, Heslington, UK
[4] Max Planck Research Group for Neuroanatomy & Connectivity, Max Planck Institute for Human Cognitive and Brain Sciences, Leipzig 04103, Germany
[5] Parietal Team, INRIA/Neurospin Saclay, France
[6] Institute of Systems Neuroscience, Heinrich-Heine University, Düsseldorf, Germany
[7] Institute of Neuroscience and Medicine (INM-1), Research Centre Jülich, 52425 Jülich, Germany
[8] Jülich Aachen Research Alliance (JARA) — Translational Brain Medicine, Aachen, Germany
[9] Department of Electrical & Systems Engineering, University of Pennsylvania, Philadelphia, PA 19104, USA
[10] Department of Psychiatry and Psychotherapy, University of Tübingen, Tübingen, Germany
[11] Department of Psychiatry, University of Heidelberg, Germany
[12] BCN Neuroimaging Center, University Medical Center Groningen, University of Groningen, Groningen, Netherlands
[13] Univ Lille, CNRS UMR9193, SCALab & CHU Lille, Fontan Hospital, CURE platform, 59000 Lille, France

* Corresponding author: danilo.bzdok@rwth-aachen.de

Short title: Default mode disturbance in schizophrenia

Keywords: Schizophrenia, default mode network, neuroimaging, functional connectivity, structural covariance, inverse covariance estimation, machine learning, sparse models

ABSTRACT

Schizophrenia is a devastating mental disease with an apparent disruption in the highly associative default mode network (DMN). Interplay between this canonical network and others probably contributes to goal-directed behavior so its disturbance is a candidate neural fingerprint underlying schizophrenia psychopathology. Previous research has reported both hyper- and hypo-connectivity within the DMN, and both increased and decreased DMN coupling with the multi-modal saliency network (SN) and dorsal attention network (DAN). The present study systematically revisited network disruption in patients with schizophrenia using data-derived network atlases and multivariate pattern-learning algorithms in a multi-site dataset (n=325). Resting-state fluctuations in unconstrained brain states were used to estimate functional connectivity, and local volume differences between individuals were used to estimate structural co-occurrence within and between the DMN, SN, and DAN. In brain structure and function, sparse inverse covariance estimates of network structure were used to characterize healthy and patients with schizophrenia groups, and to identify statistically significant group differences. Evidence did not confirm that the backbone of the DMN was the primary driver of brain dysfunction in schizophrenia. Instead, functional and structural aberrations were frequently located outside of the DMN core, such as in the anterior temporoparietal junction and precuneus. Additionally, functional covariation analyses highlighted dysfunctional DMN-DAN coupling, while structural covariation results highlighted aberrant DMN-SN coupling. Our findings highlight the role of the DMN core and its relation to canonical networks in schizophrenia and underline the importance of large-scale neural interactions as effective biomarkers and indicators of how to tailor psychiatric care to single patients.

Keywords: Schizophrenia | default mode network proper | neuroimaging | functional connectivity | structural covariance | sparse inverse covariance estimation | machine learning

INTRODUCTION

Schizophrenia is one of the most devastating medical conditions, affecting approximately 1% of the general population across cultures (Salomon et al., 2013). The clinical manifestations of schizophrenia reflect the disruption of a variety of higher-order cognitive processes (D'Argembeau et al., 2008; DeLisi, 2001; Frith and Corcoran, 1996; Haggard et al., 2003) which are likely to be subserved by the association cortex (Buckner and Krienen, 2013; Spreng et al., 2009; Stephan et al., 2016). A collection of associative cortical areas commonly linked with higher-level cognitive processes in both health and schizophrenia is the default mode network (DMN).

Several investigators have shown that dysfunction of the DMN in schizophrenia is linked to many of the positive symptoms, including delusional experiences and hallucinations, as well as negative symptoms and disorganization of thought and behavior (Bluhm et al., 2007; Camchong et al., 2009; Garrity et al., 2007; Rotarska-Jagiela et al., 2010; Whitfield-Gabrieli et al., 2009b). DMN dysregulation in schizophrenia has been associated with deficits in higher-order cognitive processes from different symptom clusters, ranging from attention to social cognition (Holt et al., 2011; Northoff and Qin, 2011; Whitfield-Gabrieli and Ford, 2012). While approximately 23% of variation in liability for schizophrenia can be explained by genetic risk variants (Lee et al., 2012; Ripke et al., 2014), evidence suggests that up to 40% of the inter-individual variance in functional connectivity patterns of the DMN is under genetic control (Glahn et al., 2010), suggesting patterns of DMN organization to be a clinically useful biomarker of schizophrenia.

Evolutionarily, regions of the association cortex, including the DMN, have increased their spatial distance from sensory-motor areas, allowing cognition to become more decoupled from perception-action cycles, a view known as the "tethering

hypothesis" (Buckner and Krienen, 2013). Indeed, the DMN was recently shown to be located at a maximum distance from sensori-motor regions in both functional and structural space (Margulies et al., 2016). These findings help explain why the DMN is particularly important for maintaining and manipulating abstract representations from downstream multi-modal brain systems (Andrews-Hanna et al., 2014; Buckner et al., 2008; Konishi et al., 2015; Raichle, 2015). Based on this *integrative* account of DMN function, its importance as a diagnostic measure for many of the features of schizophrenia may emerge through its abnormal interactions with other neural systems.

Understanding how large-scale networks subserve and control higher-order cognition is an emerging agenda in psychiatric research (Jang et al., 2017; Medaglia et al., 2015) . In particular, reorganization of the coupling modes between the DMN, saliency network (SN), and dorsal attention network (DAN) has been repeatedly proposed to carry information about the cognitive states that is complementary to task-related neural activity increases and decreases in the same network (Bzdok et al., 2016b; Margulies et al., 2016). Therefore, the present study systematically explored the dysfunctional couplings between the DMN, SN, and DAN in schizophrenia (White et al., 2010; Woodward et al., 2011). Abnormal connectivity between large-scale networks and the DMN can provide insight into the longstanding "dysconnection hypothesis" that explains schizophrenia pathophysiology as coupling impairments due to context-dependent synaptic modulation (Friston et al., 2016; Friston and Frith, 1995; Stephan et al., 2009b; Weinberger et al., 1992). According to this pathophysiological concept, interregional functional coupling might be aberrant in schizophrenia because of impaired connectional pathways. For instance, it has been proposed that the strength of dopaminergic projections between the prefrontal cortex (related to the DMN) and the DLPFC (related to the DAN) is weakened in schizophrenia (Lewis and Gonzalez-Burgos,

2006; Stephan et al., 2009a). Such dysconnection between large-scale networks may contribute to positive symptoms through the failure of attentional reallocation and monitoring processes, but also to cognitive symptoms through impaired perceptual inference and disturbance of associative learning, as well as to negative symptoms due to inability of learning from and adapting to social environments. Together, these converging lines of evidence highlight that coupling patterns between canonical networks and the DMN may be an important biomarker for many aspects of the psychopathology of schizophrenia.

Although prior studies have highlighted the DMN as important in schizophrenia, the results have revealed a multifaceted and often inconsistent picture of how this large-scale network links to the major psychiatric disorder. Several studies have reported *hypo*-connectivity between regions of the DMN, such as between the posteromedial cortex and the temporoparietal junctions (Bluhm et al., 2007; Camchong et al., 2011; Pankow et al., 2015). Other investigators instead reported *hyper*-connectivity within the DMN, such as between the medial prefrontal cortex and the posteromedial cortex (Whitfield-Gabrieli et al., 2009b; Zhou et al., 2007). Frequently inconsistent findings have also been published on pathological connectivity between the DMN and other commonly observed multi-modal networks. For example, coupling of the DMN with the DAN as well as coupling between the DMN and the SN were reported as pathologically *decreased* by some (White et al., 2010; Woodward et al., 2011) and as pathologically *increased* by others (Manoliu et al., 2013). Contradictory neural coupling findings have therefore been reported within the DMN of schizophrenia patients, as well as between the DMN and the other major brain networks including SN and DAN.

Given their intimate functional relationships and importance for disease, we studied the DMN and its pattern of coupling with the multi-modal DAN and SN in

schizophrenia adopting a comprehensive analysis strategy. First, because richer brain signals will be measured by taking into account the functional heterogeneity within the DMN at the subregional level, we deployed fine-grained topographical definitions from a recently completed DMN atlas as the regions of interest (Bzdok et al., 2016a; Bzdok et al., 2015; Bzdok et al., 2013; Eickhoff et al., 2016). Second, we extended the previous functional connectivity analyses between network parts to sparse inverse covariance estimation (Friedman et al., 2008), which has recently been adapted for use in neuroimaging (Varoquaux et al., 2010). This under-exploited statistical framework, combined with benefits of using a large data-set, (i) offered increased interpretability by removing unimportant coupling relations, (ii) acknowledged the entire set of coupling relations instead of considering only pairs in isolation, and (iii) could account for the impact of third-party influences on each coupling relation. Third, the modeling approach is sufficiently abstract to allow for analogous analyses of the relationship between networks in both the functional (resting-state connectivity) and the structural (inter-individual differences in brain volume) domain. Quantifying these aspects of structure-function correspondence underlying DMN aberration in schizophrenia aimed to complement previous connectivity investigations. We hypothesized that structural and functional interactions of DMN subnodes with two major brain networks provide insights into the mechanisms underlying schizophrenia psychopathology. That is, we expected the comparable quantification of neural network coupling in brain volume and function to allow zooming in on the multi-level disturbances underlying schizophrenia. This comprehensive analysis agenda allowed the formalization of complex correspondence between the neurobiological endo-phenotype and the clinical exo-phenotype in schizophrenia spectrum disorders.

MATERIALS AND METHODS

Data resources

This study considered magnetic resonance imaging (MRI) data from 5 different population samples acquired in Europe and USA: Aachen, Goettingen, Groeningen, Lille, and COBRE. Resting-state functional connectivity (RSFC) and voxel-based morphometric (VBM) data were collected from a total of 482 participants, 241 patients with schizophrenia and 241 healthy controls. Given the present goal to directly compare functional brain recordings and structural brain scans, we further considered only those participants who provided both RSFC and VBM in the database. These control and disease groups (n=325) were matched for age within and across sites (see Supplementary Table 1 for details). No participant in the healthy group had a record of neurological or psychiatric disorders. Each participant in the schizophrenia group had been diagnosed by a board-certified psychiatrist in accordance with the clinical criteria of the International Classification of Diseases (ICD-10) or the Diagnostic and Statistical Manual of Mental Disorders (DSM-IV-TR). All acquisition sites used 3T MRI scanners (see Supplementary Table 2 for details). For the acquisition of functional brain maps (i.e., RSFC), fMRI scans of blood-oxygen-level-dependent (BOLD) signal were recorded from the participants who were instructed to lie still during the scanning session and to let the mind wander. A post-scan interview confirmed that participants adhered to these instructions and did not fall asleep. For the acquisition of structural brain maps (i.e., VBM), 3D T1 MRI scans were recorded from each participant. All participants gave written informed consent to participate in the study, which was approved by the ethics committee of the RWTH Aachen University, Germany. Note that all phenotypic information has been anonymized for tabulation.

Brain function: Resting-state fMRI

To measure functional activity of brain regions, we analyzed resting-state EPI (echo-planar imaging) scans from standard BOLD acquisitions (see Supplementary Table 2 for details). The preprocessing was performed in SPM8 (Statistical Parametric Mapping, Wellcome Department of Imaging Neuroscience, London, UK, http://www.fil.ion.ucl.ac.uk/spm/) run under MATLAB R2014a (Mathworks, Natick, MA, US). The first 4 brain scans were discarded to allow for magnetic field saturation. The EPI images were corrected for head movement by affine registration using a 2-pass procedure. To further reduce spurious correlations induced by motion, variance that could be explained by the head motion was removed from each voxel's time series. In particular, in adherence to previously published evaluations (Chai et al., 2012; Satterthwaite et al., 2013), we removed nuisance signals according to: a) the 6 motion parameters derived from the image realignment, b) their first derivatives, and c) the respective squared terms (i.e., 24 parameter regression). These corrections have been shown to increase specificity and sensitivity of functional connectivity analyses and to detect valid signal correlation at rest. Motion correction was applied in all analyses. We did not perform global signal regression. Finally, the signal time series were band-pass filtered to preserve frequencies between 0.01 and 0.08 Hz which have previously been associated with fluctuations of neuronal activity (Fox and Raichle, 2007; Lu et al., 2007), and are least impacted by physiological artifacts such as heart rate and respirations.

Brain structure: Voxel-based morphometry MRI

To measure the local brain volume across individuals, a high-resolution anatomical image was acquired from each participant using conventional scanning sequences. Anatomical scans were preprocessed with the VBM8 toolbox

(https://dbm.neuro.uni-jena.de/vbm) in SPM8 using standard settings (DARTEL normalization to the ICBM-152 template, affine and non-linear spatial normalization). Within a unified segmentation model (Ashburner and Friston, 2005), the brain scans were corrected for bias-field inhomogeneities. The brain tissue was segmented into gray matter, white matter, and cerebrospinal fluid, while adjusting for partial volume effects. We performed nonlinear modulation of segmented images to account for the amount of expansion and contraction applied during normalization using the nonlinear only modulation function within the VBM8 toolbox. The ensuing adjusted volume measurements represented the amount of gray matter corrected for individual brain sizes.

Regions of interest

The DMN is essentially composed of four areas (which we refer to throughout as *network nodes*), including the dorsomedial prefrontal cortex (DMPFC), the posteromedial cortex (PMC), as well as the left and right temporoparietal junctions (TPJs) (Buckner et al., 2008; Raichle et al., 2001). We note that the common approach is to examine the DMN with these nodes as targets of investigation (Du et al., 2016; Greicius et al., 2003; Whitfield-Gabrieli and Ford, 2012), assuming that the nodes of the DMN are functionally homogeneous. Nevertheless, the functional contribution of each individual node to the various abstract cognitive processes maintained by the overall network remains inconclusive (cf. Andrews-Hanna et al., 2010; Bado et al., 2014; Braga and Buckner, 2017). Indeed, there is recent empirical evidence that the individual nodes of the DMN segregate into distinct subnodes (Schurz et al., 2014). These data support the notion that neurobiologically meaningful subdivisions *within* each node of the DMN

exist and could be profitably studied in the context of both healthy and abnormal human brain function.

Indeed, in a series of recent data-driven studies, the individual nodes of the DMN have been segregated into distinct subnodes based on local differences in functional interaction patterns with the rest of the brain, an established analysis technique called connectivity-based parcellation (Behrens et al., 2003; Eickhoff et al., 2015). This technique assumes that a ROI may be divided into distinct subregions based on its whole-brain connectivity profiles. For each considered DMN node, connectivity-based parcellation has previously demonstrated a subdivision of the ROI into *cluster with topographical boundary definitions* which can be reused in other studies.

Based on coherent connectivity profiles, the DMPFC was decomposed into two caudal and two rostral subnodes (Eickhoff et al., 2016). The PMC was partitioned into a ventral and dorsal subnode in the posterior cingulate cortex and one in the retrosplenial cortex and one in the precuneus (Bzdok et al., 2015). Finally, the left and right TPJs of the DMN were decomposed into an anterior and a posterior subnode (Bzdok et al., 2016a; Bzdok et al., 2013). Adopting such a fine-grained perspective on DMN organization may provide new insights into the pathophysiology of schizophrenia. These node and subnode definitions of the DMN were used as 3 different ROI sets (cf. Supplementary Table 3):

- First, we used the DMN atlas with the DMPFC, PMC, and both TPJs as composite nodes (4 ROIs), each recombining its constituent subnodes (Fig. 1.A.). The covariation analyses based on this ROI set examined the DMN at the conventional level of granularity: that is of network *nodes.* This served as a point of comparison for how this major brain network has most frequently been studied in previous brain-imaging research.

- Second, we used the full DMN atlas (12 ROIs) where the DMPFC, PMC, and the TPJs are represented as more fine-grained *subnodes* (Fig. 1.B.). The DMPFC was segregated into a left and right caudal subnode and a rostro-ventral and rostro-dorsal part (left and right cDMPFC, rvDMPFC and rdDMPFC). Note that among the midline structures of the DMN, only the DMPFC yielded a division along the right versus left hemisphere in the DMN subnode atlas. The left and right TPJs were partitioned into an anterior and posterior subnode (left and right aTPJ and pTPJ). The PMC was parcellated into 4 subnodes, including the precuneus (PREC), the ventral and dorsal posterior cingulate cortex (vPCC and dPCC), and the retrosplenial cortex (RSC). The corresponding covariation analyses examined the hypothesis that the DMN can be shown to reveal richer structure in brain signals when measured by conventional MRI scanners at the level of network *subnodes.*
- Third, the DMN subnode atlas (12 ROIs) was supplemented by nodes from two multi-modal networks (Fig. 1.C): (i) the saliency network (Bzdok et al., 2012), including the midcingulate cortex (MCC), the bilateral anterior insula (AI) and the amygdala (AM), and (ii) the dorsal attention network (Rottschy et al., 2012), including the dorsolateral prefrontal cortex (DLPFC) and the intraparietal sulcus (IPS) bilaterally (9 additional ROIs outside of the DMN). Covariation analyses examined the hypothesis that the DMN *subnodes* also display characteristic interactions with the nodes of other canonical brain networks. Indeed, the DAN and the SN have been implicated in attentional switching and reallocation of focus, processes that are markedly disrupted in schizophrenia (Luck and Gold, 2008; Maruff et al., 1996; Menon and Uddin, 2010; Potkin et al., 2009; Sato et al., 2003).

In sum, the covariation analyses of functional coupling and volumetric coupling performed in the present study were based on 3 different sets of previously established regions of interest. Collectively, the analyses are used to probe the DMN at different spatial resolutions and to systematically evaluate their relations to other major brain networks. All of the regions of interest used in this study are available online for transparency and reuse via a NeuroVault permanent link (http://neurovault.org/collections/2216/).

Signal extraction

Using the three sets of ROIs described above, quantitative measures of functional activity and grey-matter volume were extracted within the DMN, DAN, and SN ROIs in every participant. Note that all analyses were constrained to these regions of interest. For extracting relevant signal from the functional or structural brain scan, the ROIs served as topographic masks used to average the MRI signal across the voxels belonging to a given ROI. In RSFC, each target region was represented by the average BOLD signal across all voxels of that ROI. This feature-engineering strategy yielded as many functional brain variables as target regions in the ROI set for the participants. In VBM, each target region in the respective set of ROIs was represented by the average gray matter volume across all ROI voxels. Analogously, this way of engineering morphological brain features yielded as many volumetric brain variables per participant as the total number of ROIs in the current set. All ROI-wise functional or structural time series were transformed into z-scores by mean centering and unit-variance scaling. As part of the confound-removal procedure, variance that could be explained by the factors "site," "age," and "gender" as well as their two-way interactions was regressed out from the corresponding features.

Measuring network covariation: Sparse inverse covariance estimation. *Covariance* has been argued to be a key notion when estimating the statistical dependencies characteristic of small-scale neural circuits and large-scale brain networks (Horwitz et al., 1995). In the present study, we have performed formal inference of salient covariance relations in functional (i.e., RSFC) and volumetric (i.e., VBM) networks (or *graphs*, mathematically speaking) using sparse inverse covariance estimation. The automatic identification of networked organization in graphical models is an important step supporting the transition from descriptive statistics such as Pearson's correlation coefficient to generative models that capture higher-order interactions. Here, the employed statistical estimator represents an adaptation of Lasso-like regression models (Tibshirani, 1996) to Gaussian graphical models (Friedman et al., 2008), an approach that has recently been adapted for application into neuroimaging data (Varoquaux et al., 2010). The predictive validity of the derived probabilistic descriptions of the coupling properties in DMN function and volume was ascertained by cross-validation (3 folds). These schemes ensured pattern generalization by measuring the goodness of fit in unseen data as a proxy for extrapolation to the general population (Shalev-Shwartz and Ben-David, 2014). This approach facilitated model selection for hyper-parameter choice with an iteratively refined grid based on the log-likelihood score on left-out brain data (default parameters were chosen according to Varoquaux et al., 2010).

In a first step, we have computed the empirical *covariance matrix* (Fig. 2A). This simple second-order statistic reflects how strongly the times series of ROI pairs covary (in terms of functional coupling in the RSFC analysis or volumetric coupling in the VBM analysis). The empirical covariance matrix is given by

$$\hat{\Sigma}_{sample} = \frac{1}{n} \chi^T \chi,$$

where $\chi \in \mathbb{R}^{n\ x\ p}$ denotes the input dataset with p variables (i.e., functional brain signals averaged per ROI for the RSFC analysis and structural brain signals averaged per ROI for the VBM analysis) and n samples (i.e., brain scans). $\chi^T \chi$ denotes the inner product, the multiplication of the matrix χ with its transpose χ^T. The signed values in the covariance matrix indicate the direction of the linear relationship between two variables. This way of capturing the covariation in signal amplitude between any two ROIs was computed *without statistically acknowledging the possible influence from the other ROIs*. Every individual value in the covariance matrix can be viewed as a Pearson's linear correlation between each pair of ROIs, provided that the time series X were mean-centered and unit-variance scaled. Although the strengths of correlation between time series of ROI pairs were considered in isolation, these covariation strength estimates were likely to be confounded with each other. For instance, a strong influence of ROI 1 on both ROI 2 and ROI 3 would entail high estimates of covariation between ROI 2 and ROI 3. This confound in the correlation structure between any two given target regions may therefore not accurately indicate the underlying population-level interaction strength.

In a second step addressing this confound and enhancing neurobiological interpretability, we computed the partial correlations via the mathematical inverse of the covariance matrix, the so-called *precision matrix* (Fig. 2B). The optimization objective is expressed by

$$\hat{K}_{\ell 1} = argmin_{K \succ 0}\, tr(K\, \hat{\Sigma}_{sample}) - log\ det\ K + \lambda \|K\|_1,$$

where $\hat{\Sigma}_{sample}$ is the empirical covariance matrix, $\|\cdot\|_1$ denotes the regularization

constraint of putting an ℓ_1 norm on the matrix elements lying off the diagonal of the precision matrix K, and λ controls the amount of this sparsity constraint. In contrast to ordinary linear correlation matrix or to the empirical covariance matrix described above, this matrix estimates *the covariation between every two ROIs while conditioning on the potential influence of the remaining regions*. In other words, the precision matrix obtains the direct covariation between two nodes within and between the DMN, SN, and DAN by accounting for partial correlations (Marrelec et al., 2006); unlike common linear correlation approaches, it does not privilege polysynaptic coupling patterns. Coming back to our toy example, we would thus obtain the *conditionally independent proportion of covariation strength* between ROI 2 and ROI 3 that is not explained by the conjoint influence from ROI 1. Despite its utility, this statistical approach is often challenging to apply in small samples (which is particularly the case of the VBM data in the present study). In any dataset $\chi \in \mathbb{R}^{n\,x\,p}$, considerable estimation errors can arise when the number of unknown model parameters exceeds the number of samples by $n < \frac{1}{2}\, p\, (p + 1)$.

To overcome erroneous eigenstructure, statistical conditioning was improved by imposing *sparsity assumptions* by means of ℓ_1 penalization (Fig. 2C) of the inverse covariance estimation (Friedman et al., 2008; Hastie et al., 2015). In the case of multivariate Gaussian models, conditional independence between ROIs is given by the zero entries in the precision (i.e., inverse covariance) matrix. *Incorporating this frequentist prior automatically reduces the model complexity by identifying the most important pairs of network nodes and ignoring the remainder*. In the case of graphs, selecting those covariance parameters in the space of possible covariance models with sparse support (i.e., many zero-valued parameters in the graph) equates to limiting the number of graph edges. This sparse model estimation automatically balances the

compromise between biasing towards model simplicity (hence, neurobiological interpretability) and obtaining optimal model fits to brain data. The degree of ℓ_1 penalization, controlled by the coefficient λ, was evaluated and selected in the cross-validation procedure. One important consequence of ℓ_1 penalization is that searching the covariance structure reduces to a convex problem with a *unique solution*. Hence, rerunning the sparse inverse covariance estimation with different random initializations of the model parameters will yield an identical solution each time.

In sum, detailed probabilistic models of network coupling were automatically derived from multi-site brain data by using sparse inverse covariance estimation in both groups (i.e., healthy subjects and patients with schizophrenia). Models derived from RSFC data could be interpreted as summarizing the most important functional connections, while models derived from VBM data could be interpreted as summarizing the most important volumetric co-occurrence.

Testing for significant disturbance in DMN covariation

Sparse inverse covariance estimation based on RSFC and separately on VBM was to be conducted separately in the healthy group and the group of patients with schizophrenia. Separate precision matrices were thus obtained in normal controls and people with schizophrenia. Statistical significance for group differences (Fig. 2D) was assessed based on (family-wise error, multiple-comparison corrected) *p*-values for the multivariate DMN covariation based on bootstrapping for non-parametric hypothesis testing (Miller et al., 2016; Smith et al., 2015). A series of bootstrap samples (n=1000) were drawn with replacement from the healthy brain data (i.e., RSFC data for functional connectivity and VBM data for the volumetric co-occurrence). For each of the thus generated 1000 alternative dataset realizations, we performed all above steps of the

sparse inverse covariance estimation (Efron and Tibshirani, 1994). This computation generated a null distribution of possible covariation estimates for every ROI-ROI relation in healthy individuals. Bootstrapping thus provided interval estimates that indicated how each coupling strength of the DMN was expected to be distributed in the general population (Hastie et al., 2001).

Statistically significant differences between the healthy group and the group of patients with schizophrenia were then tested at the threshold corresponding to $p < 0.001$ by assessing whether the true coupling strength in individuals with schizophrenia was higher or lower than 99.9% of the coupling strengths in the healthy population. Note that, in VBM data, we have applied a more lenient threshold corresponding to $p < 0.05$, which led to statistical significance when structural covariation in schizophrenia exceeded the healthy distribution in 95% of the bootstrap samples. This is because the VBM analyses were performed in a small-sample scenario (i.e., as many brain images as participants), whereas the RSFC analyses were performed in a large-sample scenario (i.e., tens of thousands of brain images). In so doing significance testing for group differences, first in the functional covariation and then in the structural covariation, has been explicitly corrected for multiple testing, searching across all ROI pairs estimated (Miller et al., 2016; Smith et al., 2015).

RESULTS

Impact of studying nodes versus subnodes in the DMN. Based on brain measurements of functional connectivity (i.e., RSFC) in one set of analyses and structural co-occurrence (i.e., VBM) in another set of analyses, we initially examined whether subdividing traditionally studied DMN nodes into subnodes would provide richer information in brain signals. Based on 4 DMN nodes (Fig. 1.A.) versus 12 DMN subnodes (Fig. 1.B), we therefore computed sparse inverse covariance estimates (i.e., precision matrices) and their statistically significant group differences (Fig. 2).

In brain function as measured by RSFC, only the functional covariation between the right and the left temporoparietal junction (TPJ) of the DMN was determined to be significantly different between the healthy control and people with schizophrenia (Fig. 3A). We then enhanced topographical granularity. Dividing the main nodes of the DMN into their constituent subnodes confirmed the observed effect (Fig. 3B). We further observed that significant aberration did not involve the functional connectivity between the left anterior TPJ (aTPJ) and right posterior TPJ (pTPJ) subnodes. Importantly, a number of additional significant effects were not captured by the subnode-naive connectivity analyses of the DMN.

In brain structure as measured by VBM, only the structural covariation between the posteromedial cortex (PMC) and the left TPJ node was significantly different between the control and disease groups (Fig. 3C). Segmenting the composite DMN nodes into their distinct subnodes revealed that the observed effect could be more specifically credited to the morphological coupling between the left aTPJ and the precuneus (PREC) subnodes (Fig. 3D). Once more, a number of additional differences in structural covariation were observed.

These preparatory analyses converged to the conclusion that neurobiologically meaningful information contained in fMRI and MRI signals is likely to remain hidden when using a general-purpose atlas to define the human DMN. Adopting a more fine-grained subnode atlas allowed detailing previously shown and discovered new covariation effects in the DMN. This observation held true for both assessing functional coupling patterns (i.e., RSFC) and structural coupling patterns (i.e., VBM) in the DMN. Consequently, the remainder of the results section will focus on statistical analyses based on DMN subnodes.

The subsequent functional and structural covariation analyses were performed in two complementary flavors. *Intra-network* analyses performed sparse inverse covariance estimation based on the 12 subnodes from the DMN atlas (Fig. 1.B.). *Across-network* analyses performed the same multivariate modeling of network coupling but extended the 12 DMN subnodes with 9 nodes from the DAN and the SN, which are two multi-modal networks known to closely interact with the DMN (Fig. 1.C). Hence, intra-network analyses exposed the coupling differences in the DMN between healthy controls and people with schizophrenia at the subnode level. This work was extended in across-network analyses to characterize the interplay between the DMN and two other multi-modal large-scale networks.

Intra-network covariation in brain function. We systematically detailed the neural coupling fluctuations *within* the DMN in people with schizophrenia and healthy controls during the resting-state (i.e., RSFC). The functional intra-network analyses (Fig. 5 and SFig. 1 upper row) revealed the right aTPJ as the subnode with the highest number of

significantly disrupted functional connections in the DMN. 8 out of 11 connectivity targets of the right aTPJ were disturbed, including connections to three subnodes in the DMPFC, the right pTPJ, both subnodes in the left TPJ, as well as the PREC and the retrosplenial cortex (RSC). The subnode with the second highest number of functional disturbances was the rostro-dorsal DMPFC (rdDMPFC) subnode. 7 out of 11 of its connection targets were significantly affected in people with schizophrenia including the right and left caudal DMPFC (cDMPFC), the rostro-ventral DMPFC (rvDMPFC), the RSC subnode as well as both subnodes in the left TPJ and the right aTPJ. Further, the right cDMPFC and the left pTPJ subnodes in the DMN exhibited 6 out of 11 affected connections. Both shared common aberrations to the RSC, to the rdDMPFC, and to the two right TPJs as connectivity targets. Conversely, the ventral and dorsal posterior cingulate cortex (vPCC and dPCC) in the DMN showed only 2 out of 11 significantly altered functional connections to other DMN subnodes. Both were restricted to connectivity targets in the PMC.

Regarding the direction of aberrant functional coupling, the right aTPJ was hyper-connected with the left TPJs and the rvDMPFC, while it was hypo-connected toward the RSC, PREC, rdDMPFC, and left pTPJ. DMPFC subnodes were hypo-connected with each other in patients compared to the healthy group. A set of further hypo-connections were observed involving significant aberrations of the right pTPJ and the PREC with other subnodes.

In sum, multivariate connectivity analyses based on functional resting-state fluctuations illustrated statistically significant disturbances in 27 out of 60 connections between subnodes of the DMN in patients with schizophrenia. Among these, the right aTPJ exhibited the highest and the vPCC and dPCC the lowest number of affected coupling strengths with other parts of the DMN.

Across-network covariation in brain function. We then tested for group differences in the functional coupling *between* the DMN and the multi-modal networks DAN and SN (Fig. 4A; Fig. 5 and SFig. 1, second row). Importantly, after adding the nodes from the other two macroscopic brain networks for computing precision matrices, the overall pattern of covariation remained similar. In the intra-network versus across-network analyses, the differences in functional covariation between DMN subnodes were not statistically significant at $p < 0.05$ (dependent t-test). These observations support the notion that the functional connectivity patterns delineated by sparse inverse covariance estimation on RSFC data are relatively robust to changes in the size and definition of the network graph (that is, which nodes are included).

Regarding the DAN, the left intraparietal sulcus (IPS) displayed the highest number of edges that were significantly disturbed in patients. 9 out of 20 connectivity targets were affected. These included six subnodes in the DMN (rdDMPFC, dPCC, both left TPJs, right aTPJ, and PREC) and nodes in the other two networks including the mid-cingulate cortex (MCC), the right amygdala (AM) and the right IPS. The left dorsolateral prefrontal cortex (DLPFC) in the DAN also showed disrupted connectivity with 8 out of 20 targets. These included six DMN subnodes (right cDMPFC, rvDMPFC, rdDMPFC, RSC and both left TPJs) as well as nodes of the SN including the left anterior insula (AI) and MCC. The right IPS, in turn, showed seven affected connections, including DMN subnodes (rdDMPFC, left aTPJ, both right TPJs, PREC) and DAN nodes (left IPS and right DLPFC), but no part of the SN. Similar to its left-hemisphere counterpart, the right DLPFC showed six affected connections, including nodes of the SN (MCC, right AI), only one node of the DAN (right IPS), as well as several DMN subnodes (rdDMPFC, both left TPJs).

Regarding the SN, the MCC displayed 6 out of 20 functional connections disturbed in schizophrenia patients, including several DMN subnodes (left and right cDMPFC, and RSC) and nearly the entire DAN (left and right DLPFC, left IPS), but no other part of the SN. The left AI was the second most affected node with four aberrant connections, including only one DMN subnode (left cDMPFC), one DAN node (left DLPFC), and two SN nodes (right AI, left AM). The right AM in turn showed only three affected connections with the DMN (right cDMPFC, RSC) and DAN (left IPS). The right AI showed three affected connections with the DMN (dPCC), the DAN (right DLPFC), and the SN (left AI). Finally, the left AM had only two affected connections with the DMN (rvDMPFC) and the SN (left AI). As a general observation, the highest number of functional disruptions therefore appeared between the DMN and the DAN.

Regarding the directionality of functional coupling aberration, the right DLPFC of the DAN was hypo-connected with the DMN, whereas the left DLPFC and the default network were hyper-connected except with the rdDMPFC. As a similar pattern, the right IPS of the DAN was mostly hypo-connected with the DMN, except with the left aTPJ, while the left IPS was mostly hyper-connected except with the left pTPJ and the PREC. As to the SN, only the MCC and the right AM exhibited hypo-connectivities with the DMN, with the right cDMPFC and the RSC, respectively.

Summing up the present findings in functional connectivity data within and from the DMN, we made several observations. First, the right aTPJ emerged as a potential driver of perturbations to network coupling observed in schizophrenia, especially when focusing on functional covariation within the DMN (i.e., intra-network analysis). Importantly, this subnode of the DMN has been repeatedly reported not to be part of the functional core of this canonical network (Bzdok et al., 2013; Mars et al., 2012). Second, many of the subnodes, here identified to drive dysfunction in schizophrenia, are not part

of what is emerging to be a *default-mode network proper.* According to previous studies, such a stricter topographical definition of the DMN core does most likely *not* include the left and right anterior TPJs, the PREC (Bzdok et al., 2015; Margulies et al., 2009), the left and right cDMPFC (Eickhoff et al., 2016), or the RSC (Bzdok et al., 2015). Indeed, parts of the DMN core, the vPCC and dPCC, were among the least dysfunctional target regions in both intra- and across-network analyses. Third, the functional abnormalities in schizophrenia frequently manifested between commonly observed macroscopic networks, especially between the DMN and the DAN.

Intra-network covariation in brain structure. We conducted an analysis in the domain of brain structure using the VBM data that was analogous to the assessments of brain function. We thus investigated the inter-individual morphological variability within the DMN in healthy subjects and patient with schizophrenia. The structural co-occurrence results from covariation analyses on VBM data were then also evaluated for statistically significant group differences.

The structural intra-network analyses (Fig. 5 and SFig. 1, third row) revealed DMN subnodes in the PREC and the rdDMPFC as the target regions with highest structural disturbances in people with schizophrenia. For the PREC, 4 out of 11 volumetric co-occurrence relations were affected, including the medial frontal pole (rvDMPFC and rdDMPFC), dPCC, and left aTPJ. The rdDMPFC in turn showed four affected volumetric relations, including the right cDMPFC, both left TPJ subnodes, and the PREC. Conversely, only a single disturbed structural relation with other parts of the DMN was found for the right aTPJ, left cDMPFC, vPCC, and RSC.

The large majority of structural coupling aberrations were hyper-covariations between DMN subnodes. Specifically, all PMC subnodes, including the PREC, both pTPJs,

the right aTPJ and cDMPFC exhibited only hyper-covariations. Further, the left aTPJ was hypo-connected with the rdDMPFC and the right cDMPFC was hypo-connected with the rvDMPFC.

In sum, the intra-network analyses of structural co-occurrence illustrated that the DMN subnode atlas was instrumental in identifying fine-grained differences in morphological deviations in a large group of people diagnosed as schizophrenic. Healthy and diagnosed subjects showed statistically significant differences in a fifth of the volumetric coupling relations within the DMN (12 out of 60). This result stands in contrast to the higher number of functional aberrations found in the corresponding analyses in the functional imaging arm of the study (RSFC).

Across-network covariation in brain structure. We finally tested for group differences in structural covariation *between* the DMN and the DAN and SN (Fig. 4.B.; Fig. 5 and SFig. 1, lowest row). Concurrent with the functional covariation analyses, the overall pattern of structural coupling was similar when computing the precision matrices after taking into account the nodes of the DAN and SN. In the intra-network versus across-network analyses, the differences in structural covariation between DMN subnodes were not statistically significant at $p < 0.05$ (dependent t-test). As another global observation, none of the structural analyses showed any negative covariation in the healthy or disease group, in contrast to the various positive and negative coupling results observed in the functional covariation analyses. Moreover, we again showed a lower overall number of statistically significant volume differences in people with schizophrenia (31 significant abnormalities) compared to the corresponding group differences in brain function (61 significant abnormalities).

Regarding the DAN, we identified the left DLPFC as exhibiting statistically significant differences between healthy controls and people with schizophrenia in 3 out of 20 volumetric relations. These included the right aTPJ, MCC and right AI. Congruently, the DLPFC in the right hemisphere also exhibited affected volumetric relations with the right aTPJ and the right AI. Further, the right and left IPS both showed impaired volumetric coupling with the AM of the same hemisphere. While the right IPS was also disrupted in its volumetric relation with the MCC, the left IPS displayed another impaired relation with the left cDMPFC.

Regarding the SN, the MCC as well as left and right AI of this same commonly observed multi-modal network showed the highest number of impaired volumetric couplings (besides rvDMPFC). All three SN nodes showed disturbed relations with subnodes in the DMPFC. More specifically, left AI exhibited 4 affected relations, including the right cDMPFC, the rvDMPFC, the vPCC, the left pTPJ, and the right AI. The AI in the right hemisphere instead showed affected relations with rvDMPFC, left AI, left AM, as well as the right and left DLPFC. The MCC had 5 affected volumetric relations including the rdDMPFC, the PREC, the left DLPFC, as well as the IPS and pTPJ in the right hemisphere. Finally, both AM showed dysfunctional structural coupling among each other as well as to the IPS in the same hemisphere, while the left AM showed additional abnormalities with the right AI and the left pTPJ. As a general observation, the highest number of structural disruptions emerged between the DMN and the SN.

Consistent with the intra-network analysis in brain structure, patients mostly exhibited significant hyper-covariations between the DMN and the other canonical networks. Specifically, both the MCC and the right AI, the most disrupted SN nodes towards the DMN, exhibited only hyper-covariations while the SN exhibited hypo-covariations with the DMN only from the left AM and the right AI.

In sum, major brain networks, such as the DAN and SN, demonstrated specific volumetric coupling relations with distinct subnodes of the DMN that were shown to be impaired in schizophrenia. Importantly, only a few subnodes of the DMN proper showed statistically significant group differences. Similar to the present finding in brain function, the morphological properties of the DMN proper were found to be more intact than many other parts of the graph. Moreover, nodes of the SN were most impaired among all three networks and featured most aberrations with coupling partners of the DMN proper.

DISCUSSION

Our study suggests that dysconnectivity and dysregulation anchored in the default mode network is a neurobiological hallmark of schizophrenia spectrum disorders. Adopting a systems neuroscience approach, we aimed at reconciling coupling within the highly associative DMN and its coupling with the multi-modal saliency and dorsal attention networks. We combined meta-analytically defensible network definitions and recently developed machine learning methods for multivariate discovery of primary covariation patterns. Network coupling was investigated in two domains, first, based on brain measurements of functional resting-state fluctuations (i.e., RSFC) and second, based on structural brain morphology (i.e., VBM). Applying an identical modeling strategy to observed functional fluctuations and volumetric differences facilitated conclusions across neurobiological levels, including their third-party coupling influences. Functional covariation analyses revealed extended disturbances related to the right anterior temporoparietal junction and the DAN. In contrast, structural covariation analyses emphasized disturbances related to the precuneus in the posteromedial cortex and the SN. These findings emphasize disturbed coupling between the DMN and other large-scale networks rather than exclusive dysregulation of core parts within the DMN. Collectively, our results suggest that some previously inconsistent findings may be reconciled by using a DMN atlas with subnode resolution to recover currently under-appreciated, physiologically meaningful covariation patterns in schizophrenia.

Covariation patterns mostly altered by cortical areas that are not part of the "DMN proper". Covariation analyses applied to resting-state fluctuations within and from the DMN identified the right anterior TPJ subnode as featuring a particularly high number of

coupling perturbations in people diagnosed as schizophrenic, especially in the functional intra-network analyses. Recent brain parcellation studies have associated the anterior portions of the TPJs with externally focused evaluation of visual, auditory, tactile, and other preprocessed sensory input as well as maintenance of perception-action cycles associated with the SN (Bzdok et al., 2016a; Bzdok et al., 2013; Glasser et al., 2015; Humphreys and Ralph, 2015; Mars et al., 2012). Hence, the present investigation at subnode resolution points to an aberration of multi-modal integration of perception-action cycles, more closely linked to DAN and SN function, rather than to imagination-based thought processes, more closely linked to DMN function (Hassabis et al., 2007; Wang et al., 2017). This quantitative evidence potentially relates to several clinical manifestations of schizophrenia, such as false subjective beliefs (delusion), perceiving unreal stimuli (hallucinations), awkward sensations (paresthesia), concentration difficulties, as well as disorganized speech and motor movement.

Across structural covariation analyses, the PREC emerged as one of the most impaired DMN nodes. The PREC is anatomically located in the parietal lobe and is thought to subserve visuomotor processes, such as those necessary for attentional shifting, reaching movements, and hand-eye coordination (Margulies et al., 2009; Mesulam, 1981; Stephan et al., 1995). These cognitive associations ascribed to the PREC can indeed be related to several schizophrenia symptoms, especially loss of train of thought, impairments in executive function, working memory, and memory retrieval, as well as psychogenic motor abnormalities (catatonia). Both anterior TPJs and the PREC are similarly believed to govern context-dependent reorganization of large-scale networks (Bzdok et al., 2013; Cavanna and Trimble, 2006; Downar et al., 2000; Seghier, 2013).

As a general conclusion, functional and structural findings agreed in emphasizing that (i) the communication within the medial core of the DMN in prefrontal and cingulate regions was relatively preserved in the examined patients and (ii) the dysfunction of schizophrenia substantially involves subnodes that do not belong to what is emerging to be a *default-mode network proper.* Such a stricter topographical definition of the DMN excludes the anterior left and right TPJ, the PREC (Bzdok et al., 2015; Margulies et al., 2009), the retrosplenial cortex closer to the limbic system (Braga and Buckner, 2017; Bzdok et al., 2015; Vogt and Laureys, 2005), and the caudal DMPFCs closer to the anterior cingulate cortex (Eickhoff et al., 2016; Vogt and Pandya, 1987). Instead, a definition of the DMN core includes the ventral and the dorsal PCCs, the left and right posterior TPJs, and the rostroventral and rostrodorsal DMPFC. Both the ventral and dorsal PCCs were identified among the least dysfunctional areas across all present analyses.

Collectively, these data suggest that dysfunctions in the DMN that underpin schizophrenic pathology do not emerge from the core of the network, but are reflected in the coupling of the subnodes of the larger network, regions that prior work has implicated as participating in large-scale networks other than the DMN. In particular, our study highlights disturbed inter-network communication, focused on the right anterior TPJ and PREC, as candidate drivers of the disease process that underpins schizophrenia.

Discrepancies between volumetric and functional aberration patterns in schizophrenia. In the context of schizophrenia, network analyses have frequently been performed on either functional brain measurements (Liu et al., 2008; Lynall et al., 2010; Yu et al., 2013) or structural brain measurements (Konrad and Winterer, 2008; van den

Heuvel et al., 2010). Direct investigations of the volume-function correspondence in long-distance coupling have been less frequent (But see: Clos et al., 2014; Honey et al., 2009; Kelly et al., 2012).

The present study departs from previous single-modality investigations by applying identical covariation analyses to RSFC and VBM data to facilitate neurobiological conclusions independent of differences in the employed statistical models. We did not find strong evidence that these domains show analogous patterns when considering the DMN in isolation or its interplay with the DAN and SN. In the functional domain, for instance, the right anterior TPJ was the overall most affected subnode, while the PREC and the right dorsal DMPFC exhibited the strongest disruptions in the structural domain. These findings suggest that neural disturbances in schizophrenia are a result of heterogeneous changes in cortex architecture that do not map in a simple way to patterns of neural communication. In addition, these regularities emphasize abnormalities in schizophrenia *between* networks rather than *within* the DMN core.

Given that the DMN is believed to exert control over the subordinate DAN and SN (Carhart-Harris and Friston, 2010; Margulies et al., 2016), it is exciting that our results revealed a dissociation in their disrupted links in the structural and functional network analyses. DMN interactions with the SN were more consistently altered in brain morphology (VBM), whereas DMN interactions with the DAN emerged as more consistently altered in brain function (RSFC) in patients with schizophrenia. Congruently, previous quantitative meta-analysis on schizophrenia and other psychiatric populations highlighted aberration in the SN across volumetric neuroimaging studies (Goodkind et al., 2015) and dysfunction in the DAN in large amounts of functional neuroimaging studies (McTeague et al., 2017). Both inter-

individual differences in local brain volume (e.g., Draganski et al., 2004) and fluctuations in resting-state patterns (e.g., Rosenberg et al., 2015) have been shown to offer reliable correlates of success and failure in specific cognitive performances (Kanai and Rees, 2011). Differences in the executive control performance between healthy individuals were related to cortical thickness differences in the SN extending into parts of the DMN (Westlye et al., 2011). The present pathological increases in structural DMN-SN coupling may therefore provide insight into a longer-term compensatory mechanism due to impaired executive function in patients with schizophrenia. In contrast, the present patterns of pathological increases and decreases in functional DMN-DAN coupling may uncover a multifaceted dysbalance in allocating attentional resources to internal thought and emotion (cf. Shim et al., 2010; Whitfield-Gabrieli et al., 2009a). Thus, previous isolated findings are reconciled by our across-modal approach that situated detailed disruption patterns in the context of top-level DMN control on intermediate multi-modal networks.

Although we did not find a close mapping between structure and function, in both domains we found evidence that corroborates the dysconnection hypothesis of schizophrenia (Friston et al., 2016; Friston and Frith, 1995; Stephan et al., 2009b; Weinberger et al., 1992) as a central pathophysiological component that could underlie schizophrenia spectrum disorders. Together, our findings support an account of the pathophysiology of schizophrenia in which abnormal integrity of long-range connections prevent integration of information from systems that support the maintenance of cognitive sets, such as mediated by the SN, or the dynamic allocation of cognitive resources, such as mediated by the DAN (Dosenbach et al., 2006; Seeley et al., 2007).

Future directions. More globally, the overwhelming majority of mental disorders are known to show disturbance of the DMN (Broyd et al., 2009; Whitfield-Gabrieli and Ford, 2012). Yet, we deem it unlikely that brain disorders with diverging clinical phenotypes are caused by identical neurobiological disease mechanisms. Rather, the numerous brain disorders affecting the DMN are perhaps more realistically framed to underlie a stratification of partly overlapping pathophysiologies (cf. Calhoun et al., 2011; Meda et al., 2012; Öngür et al., 2010). Investigating the DMN at an increased level of topographic granularity may be a prerequisite for identifying the DMN dysregulation specific to each major psychiatric disorder. A variety of neurobiologically distinct types of DMN aberration may expose brain phenotypes that enable effective stratification of patients with schizophrenia in clinical practice (Brodersen et al., 2011). If successful in schizophrenia, the present analysis framework may scale to other major psychiatric disorders.

Moreover, the sparse inverse covariation approach has several advantages, including enhanced interpretability, statistically privileging direct network influences, and inter-operability across different brain-imaging modalities. However, the employed statistical model is inherently blind to interaction partners outside of the network graph and disregards higher-order interaction between the nodes in the network graph (Ganmor et al., 2011; Giusti et al., 2016; Giusti et al., 2015). That is, our analysis strategy was able to consider all targeted inter-nodal relations simultaneously but assumed network interaction to be only composed of a set of dyadic partners. Going beyond pair-wise covariation in network analysis would be an exciting future extension of the present work (Bassett and Sporns, 2017).

Conclusion. Conventional brain-imaging measurements of the highly associative DMN were shown to carry fine-grained information about its coupling relation to other macroscopic brain networks. We could thus conclude that schizophrenia may not be explained by a primary dysfunction in the backbone of the DMN ("default-mode proper"). Schizophrenia psychopathology may not only be due to deficits *within* the DMN but especially also to deficits *between* the DMN and other multi-modal networks including the SN and DAN. Further, by leveraging state-of-the-art machine learning techniques for a direct juxtaposition of functional and structural covariation patterns, we provide empirical evidence for complementary disease mechanisms in schizophrenia patients. These first steps towards a more integrative approach to study DMN disturbance may be critical to chisel out the "dysconnection" pathophysiology potentially underlying schizophrenia.

ACKNOWLEDGEMENTS. Dr. Bzdok is funded by the Deutsche Forschungsgemeinschaft (DFG, BZ2/2-1, BZ2/3-1, and BZ2/4-1; International Research Training Group IRTG2150), Amazon AWS Research Grant (2016 and 2017), the German National Merit Foundation, and the START-Program of the Faculty of Medicine, RWTH Aachen. Dr. Bassett acknowledges support from the John D. and Catherine T. MacArthur Foundation, the Alfred P. Sloan Foundation, the Army Research Laboratory and the Army Research Office through contract numbers W911NF-10-2-0022 and W911NF-14-1-0679, the National Institute of Mental Health (2R01-DC-009209-11), the National Institute of Child Health and Human Development (1R01HD086888-01), the Office of Naval Research, and the National Science Foundation (BCS-1441502, BCS-1430087, NSF PHY-1554488). Dr. Margulies and Dr. Smallwood received support from the Welcome Trust 103817/Z/14/Z and from the Volkswagen Foundation (Wandering Minds – 89440 and 89439). Dr. Smallwood was further supported by the European Research Council (WANDERINGMINDS–646927).

BIBLIOGRAPHY

Abraham A, Pedregosa F, Eickenberg M, Gervais P, Mueller A, Kossaifi J, Gramfort A, Thirion B, Varoquaux G. (2014): Machine learning for neuroimaging with scikit-learn. Front Neuroinform 8:14.

Andrews-Hanna JR, Reidler JS, Sepulcre J, Poulin R, Buckner RL. (2010): Functional-anatomic fractionation of the brain's default network. Neuron 65(4):550-62.

Andrews‐Hanna JR, Smallwood J, Spreng RN. (2014): The default network and self‐generated thought: component processes, dynamic control, and clinical relevance. Annals of the New York Academy of Sciences 1316(1):29-52.

Ashburner J, Friston KJ. (2005): Unified segmentation. Neuroimage 26(3):839-51.

Bado P, Engel A, Oliveira‐Souza R, Bramati IE, Paiva FF, Basilio R, Sato JR, Tovar‐Moll F, Moll J. (2014): Functional dissociation of ventral frontal and dorsomedial default mode network components during resting state and emotional autobiographical recall. Human brain mapping 35(7):3302-3313.

Bassett DS, Sporns O. (2017): Network neuroscience. Nature Neuroscience 20(3):353-364.

Behrens TE, Johansen-Berg H, Woolrich MW, Smith SM, Wheeler-Kingshott CA, Boulby PA, Barker GJ, Sillery EL, Sheehan K, Ciccarelli O and others. (2003): Non-invasive mapping of connections between human thalamus and cortex using diffusion imaging. Nat Neurosci 6(7):750-7.

Bluhm RL, Miller J, Lanius RA, Osuch EA, Boksman K, Neufeld RWJ, Théberge J, Schaefer B, Williamson P. (2007): Spontaneous low-frequency fluctuations in the BOLD signal in schizophrenic patients: anomalies in the default network. Schizophrenia bulletin 33(4):1004-1012.

Braga RM, Buckner RL. (2017): Parallel interdigitated distributed networks within the individual estimated by intrinsic functional connectivity. Neuron 95(2):457-471. e5.

Brodersen KH, Schofield TM, Leff AP, Ong CS, Lomakina EI, Buhmann JM, Stephan KE. (2011): Generative embedding for model-based classification of fMRI data. PLoS Comput Biol 7(6):e1002079.

Broyd SJ, Demanuele C, Debener S, Helps SK, James CJ, Sonuga-Barke EJ. (2009): Default-mode brain dysfunction in mental disorders: a systematic review. Neuroscience & biobehavioral reviews 33(3):279-296.

Buckner RL, Andrews‐Hanna JR, Schacter DL. (2008): The brain's default network. Annals of the New York Academy of Sciences 1124(1):1-38.

Buckner RL, Krienen FM. (2013): The evolution of distributed association networks in the human brain. Trends in Cognitive Sciences 17(12):648-665.

Bzdok D, Hartwigsen G, Reid A, Laird AR, Fox PT, Eickhoff SB. (2016a): Left inferior parietal lobe engagement in social cognition and language. Neuroscience & Biobehavioral Reviews.

Bzdok D, Heeger A, Langner R, Laird AR, Fox PT, Palomero-Gallagher N, Vogt BA, Zilles K, Eickhoff SB. (2015): Subspecialization in the human posterior medial cortex. Neuroimage 106:55-71.

Bzdok D, Langner R, Schilbach L, Jakobs O, Roski C, Caspers S, Laird AR, Fox PT, Zilles K, Eickhoff SB. (2013): Characterization of the temporo-parietal junction by combining data-driven parcellation, complementary connectivity analyses, and functional decoding. Neuroimage 81:381-392.

Bzdok D, Schilbach L, Vogeley K, Schneider K, Laird AR, Langner R, Eickhoff SB. (2012): Parsing the neural correlates of moral cognition: ALE meta-analysis on morality, theory of mind, and empathy. Brain Structure and Function 217(4):783-796.

Bzdok D, Varoquaux G, Grisel O, Eickenberg M, Poupon C, Thirion B. (2016b): Formal models of the network co-occurrence underlying mental operations. PLoS Comput Biol 12(6):e1004994.

Calhoun VD, Sui J, Kiehl K, Turner J, Allen E, Pearlson G. (2011): Exploring the psychosis functional connectome: aberrant intrinsic networks in schizophrenia and bipolar disorder. Magnetic resonance imaging of disturbed brain connectivity in psychiatric illness:35.

Camchong J, Lim KO, Sponheim SR, MacDonald Iii AW. (2009): Frontal white matter integrity as an endophenotype for schizophrenia: diffusion tensor imaging in monozygotic twins and patients' nonpsychotic relatives. Frontiers in human neuroscience 3:35.

Camchong J, MacDonald AW, Bell C, Mueller BA, Lim KO. (2011): Altered functional and anatomical connectivity in schizophrenia. Schizophrenia bulletin 37(3):640-650.

Carhart-Harris RL, Friston KJ. (2010): The default-mode, ego-functions and free-energy: a neurobiological account of Freudian ideas. Brain:awq010.

Cavanna AE, Trimble MR. (2006): The precuneus: a review of its functional anatomy and behavioural correlates. Brain 129(Pt 3):564-83.

Chai XJ, Castanon AN, Ongur D, Whitfield-Gabrieli S. (2012): Anticorrelations in resting state networks without global signal regression. Neuroimage 59(2):1420-8.

Clos M, Rottschy C, Laird AR, Fox PT, Eickhoff SB. (2014): Comparison of structural covariance with functional connectivity approaches exemplified by an investigation of the left anterior insula. NeuroImage 99:269-280.

D'Argembeau A, Raffard S, Van der Linden M. (2008): Remembering the past and imagining the future in schizophrenia. Journal of abnormal psychology 117(1):247.

DeLisi LE. (2001): Speech disorder in schizophrenia: Review of the literature and exploration of its relation to the uniquely human capacity for language. Schizophrenia Bulletin 27(3):481.

Dosenbach NU, Visscher KM, Palmer ED, Miezin FM, Wenger KK, Kang HC, Burgund ED, Grimes AL, Schlaggar BL, Petersen SE. (2006): A core system for the implementation of task sets. Neuron 50(5):799-812.

Downar J, Crawley AP, Mikulis DJ, Davis KD. (2000): A multimodal cortical network for the detection of changes in the sensory environment. Nat Neurosci 3(3):277-283.

Draganski B, Gaser C, Busch V, Schuierer G, Bogdahn U, May A. (2004): Neuroplasticity: changes in grey matter induced by training. Nature 427(6972):311-312.

Du Y, Pearlson GD, Yu Q, He H, Lin D, Sui J, Wu L, Calhoun VD. (2016): Interaction among subsystems within default mode network diminished in schizophrenia patients: A dynamic connectivity approach. Schizophrenia research 170(1):55-65.

Efron B, Tibshirani RJ. 1994. An introduction to the bootstrap: CRC press.

Eickhoff SB, Laird AR, Fox PT, Bzdok D, Hensel L. (2016): Functional Segregation of the Human Dorsomedial Prefrontal Cortex. Cereb Cortex 26(1):304-21.

Eickhoff SB, Thirion B, Varoquaux G, Bzdok D. (2015): Connectivity‐based parcellation: Critique and implications. Human brain mapping 36(12):4771-4792.

Fox MD, Raichle ME. (2007): Spontaneous fluctuations in brain activity observed with functional magnetic resonance imaging. Nature Reviews Neuroscience 8(9):700-711.

Friedman J, Hastie T, Tibshirani R. (2008): Sparse inverse covariance estimation with the graphical lasso. Biostatistics 9(3):432-441.

Friston K, Brown HR, Siemerkus J, Stephan KE. (2016): The dysconnection hypothesis (2016). Schizophrenia Research.

Friston KJ, Frith CD. (1995): Schizophrenia - a disconnection syndrome. Clin. Neurosci. 3:89-97.

Frith CD, Corcoran R. (1996): Exploring 'theory of mind'in people with schizophrenia. Psychological medicine 26(03):521-530.

Ganmor E, Segev R, Schneidman E. (2011): Sparse low-order interaction network underlies a highly correlated and learnable neural population code. Proceedings of the National Academy of Sciences 108(23):9679-9684.

Gao JS, Huth AG, Lescroart MD, Gallant JL. (2015): Pycortex: an interactive surface visualizer for fMRI. Frontiers in neuroinformatics 9:23.

Garrity AG, Pearlson GD, McKiernan K, Lloyd D, Kiehl KA, Calhoun VD. (2007): Aberrant "default mode" functional connectivity in schizophrenia. American journal of psychiatry.

Giusti C, Ghrist R, Bassett DS. (2016): Two's company, three (or more) is a simplex. Journal of Computational Neuroscience:1-14.

Giusti C, Pastalkova E, Curto C, Itskov V. (2015): Clique topology reveals intrinsic geometric structure in neural correlations. Proceedings of the National Academy of Sciences 112(44):13455-13460.

Glahn DC, Winkler AM, Kochunov P, Almasy L, Duggirala R, Carless MA, Curran JC, Olvera RL, Laird AR, Smith SM and others. (2010): Genetic control over the resting brain. PNAS 107(3):1223-8.

Glasser MF, Coalson T, Robinson E, Hacker C, Harwell J, Yacoub E, Ugurbil K, Anderson J, Beckmann CF, Jenkinson M. (2015): A Multi-modal parcellation of human cerebral cortex. Nature.

Goodkind M, Eickhoff SB, Oathes DJ, Jiang Y, Chang A, Jones-Hagata LB, Ortega BN, Zaiko YV, Roach EL, Korgaonkar MS and others. (2015): Identification of a Common Neurobiological Substrate for Mental Illness. JAMA Psychiatry.

Greicius MD, Krasnow B, Reiss AL, Menon V. (2003): Functional connectivity in the resting brain: a network analysis of the default mode hypothesis. Proceedings of the National Academy of Sciences 100(1):253-258.

Haggard P, Martin F, Taylor-Clarke M, Jeannerod M, Franck N. (2003): Awareness of action in schizophrenia. Neuroreport 14(7):1081-1085.

Hassabis D, Kumaran D, Maguire EA. (2007): Using imagination to understand the neural basis of episodic memory. J Neurosci 27(52):14365-74.

Hastie T, Tibshirani R, Friedman J. 2001. The Elements of Statistical Learning. Heidelberg, Germany: Springer Series in Statistics.

Hastie T, Tibshirani R, Wainwright M. 2015. Statistical Learning with Sparsity: The Lasso and Generalizations: CRC Press.

Holt DJ, Cassidy BS, Andrews-Hanna JR, Lee SM, Coombs G, Goff DC, Gabrieli JD, Moran JM. (2011): An anterior-to-posterior shift in midline cortical activity in schizophrenia during self-reflection. Biological psychiatry 69(5):415-423.

Honey CJ, Sporns O, Cammoun L, Gigandet X, Thiran JP, Meuli R, Hagmann P. (2009): Predicting human resting-state functional connectivity from structural connectivity. Proc Natl Acad Sci U S A 106(6):2035-40.

Horwitz B, McIntosh A, Haxby J, Grady C. (1995): Network analysis of brain cognitive function using metabolic and blood flow data. Behavioural brain research 66(187).

Humphreys GF, Ralph MAL. (2015): Fusion and fission of cognitive functions in the human parietal cortex. Cerebral Cortex 25(10):3547-3560.
Jang C, Knight EQ, Pae C, Park B, Yoon S-A, Park H-J. (2017): Individuality manifests in the dynamic reconfiguration of large-scale brain networks during movie viewing. Scientific reports 7.
Kanai R, Rees G. (2011): The structural basis of inter-individual differences in human behaviour and cognition. Nat Rev Neurosci 12(4):231-42.
Kelly C, Toro R, Di Martino A, Cox CL, Bellec P, Castellanos FX, Milham MP. (2012): A convergent functional architecture of the insula emerges across imaging modalities. Neuroimage 61(4):1129-1142.
Konishi M, McLaren DG, Engen H, Smallwood J. (2015): Shaped by the past: the default mode network supports cognition that is independent of immediate perceptual input. PloS one 10(6):e0132209.
Konrad A, Winterer G. (2008): Disturbed structural connectivity in schizophrenia—primary factor in pathology or epiphenomenon? Schizophrenia bulletin 34(1):72-92.
Lee SH, DeCandia TR, Ripke S, Yang J, Sullivan PF, Goddard ME, Keller MC, Visscher PM, Wray NR, Consortium SPG-WAS. (2012): Estimating the proportion of variation in susceptibility to schizophrenia captured by common SNPs. Nature genetics 44(3):247-250.
Lewis DA, Gonzalez-Burgos G. (2006): Pathophysiologically based treatment interventions in schizophrenia. Nature medicine 12(9):1016-1022.
Liu Y, Liang M, Zhou Y, He Y, Hao Y, Song M, Yu C, Liu H, Liu Z, Jiang T. (2008): Disrupted small-world networks in schizophrenia. Brain 131(4):945-961.
Lu H, Zuo Y, Gu H, Waltz JA, Zhan W, Scholl CA, Rea W, Yang Y, Stein EA. (2007): Synchronized delta oscillations correlate with the resting-state functional MRI signal. Proceedings of the National Academy of Sciences 104(46):18265-18269.
Luck SJ, Gold JM. (2008): The construct of attention in schizophrenia. Biological psychiatry 64(1):34-39.
Lynall M-E, Bassett DS, Kerwin R, McKenna PJ, Kitzbichler M, Muller U, Bullmore E. (2010): Functional connectivity and brain networks in schizophrenia. The Journal of Neuroscience 30(28):9477-9487.
Manoliu A, Riedl V, Zherdin A, Mühlau M, Schwerthöffer D, Scherr M, Peters H, Zimmer C, Förstl H, Bäuml J. (2013): Aberrant dependence of default mode/central executive network interactions on anterior insular salience network activity in schizophrenia. Schizophrenia bulletin:sbt037.
Margulies DS, Ghosh SS, Goulas A, Falkiewicz M, Huntenburg JM, Langs G, Bezgin G, Eickhoff SB, Castellanos FX, Petrides M. (2016): Situating the default-mode network along a principal gradient of macroscale cortical organization. Proceedings of the National Academy of Sciences 113(44):12574-12579.
Margulies DS, Vincent JL, Kelly C, Lohmann G, Uddin LQ, Biswal BB, Villringer A, Castellanos FX, Milham MP, Petrides M. (2009): Precuneus shares intrinsic functional architecture in humans and monkeys. Proc Natl Acad Sci U S A 106(47):20069-74.
Marrelec G, Krainik A, Duffau H, Pelegrini-Issac M, Lehericy S, Doyon J, Benali H. (2006): Partial correlation for functional brain interactivity investigation in functional MRI. Neuroimage 32(1):228-37.
Mars RB, Sallet J, Schüffelgen U, Jbabdi S, Toni I, Rushworth MFS. (2012): Connectivity-based subdivisions of the human right "temporoparietal junction area": evidence

for different areas participating in different cortical networks. Cerebral cortex 22(8):1894-1903.
Maruff P, Pantelis C, Danckert J, Smith D, Currie J. (1996): Deficits in the endogenous redirection of covert visual attention in chronic schizophrenia. Neuropsychologia 34(11):1079-1084.
McTeague LM, Huemer J, Carreon DM, Jiang Y, Eickhoff SB, Etkin A. (2017): Identification of Common Neural Circuit Disruptions in Cognitive Control Across Psychiatric Disorders. American Journal of Psychiatry:appi. ajp. 2017.16040400.
Meda SA, Gill A, Stevens MC, Lorenzoni RP, Glahn DC, Calhoun VD, Sweeney JA, Tamminga CA, Keshavan MS, Thaker G. (2012): Differences in resting-state functional magnetic resonance imaging functional network connectivity between schizophrenia and psychotic bipolar probands and their unaffected first-degree relatives. Biological psychiatry 71(10):881-889.
Medaglia JD, Lynall M-E, Bassett DS. (2015): Cognitive network neuroscience. Journal of cognitive neuroscience.
Menon V, Uddin LQ. (2010): Saliency, switching, attention and control: a network model of insula function. Brain Structure and Function 214(5-6):655-667.
Mesulam MM. (1981): A cortical network for directed attention and unilateral neglect. Ann Neurol 10(4):309-25.
Miller KL, Alfaro-Almagro F, Bangerter NK, Thomas DL, Yacoub E, Xu J, Bartsch AJ, Jbabdi S, Sotiropoulos SN, Andersson JLR. (2016): Multimodal population brain imaging in the UK Biobank prospective epidemiological study. Nature Neuroscience.
Northoff G, Qin P. (2011): How can the brain's resting state activity generate hallucinations? A 'resting state hypothesis' of auditory verbal hallucinations. Schizophrenia research 127(1):202-214.
Öngür D, Lundy M, Greenhouse I, Shinn AK, Menon V, Cohen BM, Renshaw PF. (2010): Default mode network abnormalities in bipolar disorder and schizophrenia. Psychiatry Research: Neuroimaging 183(1):59-68.
Pankow A, Deserno L, Walter M, Fydrich T, Bermpohl F, Schlagenhauf F, Heinz A. (2015): Reduced default mode network connectivity in schizophrenia patients. Schizophrenia research 165(1):90-93.
Potkin S, Turner J, Brown G, McCarthy G, Greve D, Glover G, Manoach D, Belger A, Diaz M, Wible C. (2009): Working memory and DLPFC inefficiency in schizophrenia: the FBIRN study. Schizophrenia bulletin 35(1):19-31.
Raichle ME. (2015): The brain's default mode network. Annual review of neuroscience 38:433-447.
Raichle ME, MacLeod AM, Snyder AZ, Powers WJ, Gusnard DA, Shulman GL. (2001): A default mode of brain function. PNAS 98(2):676-82.
Ripke S, Neale BM, Corvin A, Walters JT, Farh K-H, Holmans PA, Lee P, Bulik-Sullivan B, Collier DA, Huang H. (2014): Biological insights from 108 schizophrenia-associated genetic loci. Nature 511(7510):421.
Rosenberg MD, Finn ES, Scheinost D, Papademetris X, Shen X, Constable RT, Chun MM. (2015): A neuromarker of sustained attention from whole-brain functional connectivity. Nature neuroscience.
Rotarska-Jagiela A, van de Ven V, Oertel-Knöchel V, Uhlhaas PJ, Vogeley K, Linden DE. (2010): Resting-state functional network correlates of psychotic symptoms in schizophrenia. Schizophrenia research 117(1):21-30.
Rottschy C, Langner R, Dogan I, Reetz K, Laird AR, Schulz JB, Fox PT, Eickhoff SB. (2012): Modelling neural correlates of working memory: a coordinate-based meta-analysis. Neuroimage 60(1):830-846.

Salomon JA, Vos T, Hogan DR, Gagnon M, Naghavi M, Mokdad A, Begum N, Shah R, Karyana M, Kosen S. (2013): Common values in assessing health outcomes from disease and injury: disability weights measurement study for the Global Burden of Disease Study 2010. The Lancet 380(9859):2129-2143.

Sato Y, Yabe H, Todd J, Michie P, Shinozaki N, Sutoh T, Hiruma T, Nashida T, Matsuoka T, Kaneko S. (2003): Impairment in activation of a frontal attention-switch mechanism in schizophrenic patients. Biological psychology 62(1):49-63.

Satterthwaite TD, Elliott MA, Gerraty RT, Ruparel K, Loughead J, Calkins ME, Eickhoff SB, Hakonarson H, Gur RC, Gur RE and others. (2013): An improved framework for confound regression and filtering for control of motion artifact in the preprocessing of resting-state functional connectivity data. Neuroimage 64:240-56.

Schurz M, Radua J, Aichhorn M, Richlan F, Perner J. (2014): Fractionating theory of mind: A meta-analysis of functional brain imaging studies. Neuroscience & Biobehavioral Reviews 42:9-34.

Seeley WW, Menon V, Schatzberg AF, Keller J, Glover GH, Kenna H, Reiss AL, Greicius MD. (2007): Dissociable intrinsic connectivity networks for salience processing and executive control. J Neurosci 27(9):2349-56.

Seghier ML. (2013): The Angular Gyrus: Multiple Functions and Multiple Subdivisions. Neuroscientist:43-61.

Shalev-Shwartz S, Ben-David S. 2014. Understanding machine learning: From theory to algorithms: Cambridge University Press.

Shim G, Oh JS, Jung WH, Jang JH, Choi C-H, Kim E, Park H-Y, Choi J-S, Jung MH, Kwon JS. (2010): Altered resting-state connectivity in subjects at ultra-high risk for psychosis: an fMRI study. Behavioral and Brain Functions 6(1):58.

Smith SM, Nichols TE, Vidaurre D, Winkler AM, Behrens TEJ, Glasser MF, Ugurbil K, Barch DM, Van Essen DC, Miller KL. (2015): A positive-negative mode of population covariation links brain connectivity, demographics and behavior. Nat Neurosci 18(11):1565-1567.

Spreng RN, Mar RA, Kim ASN. (2009): The common neural basis of autobiographical memory, prospection, navigation, theory of mind, and the default mode: a quantitative meta-analysis. Journal of cognitive neuroscience 21(3):489-510.

Stephan KE, Binder EB, Breakspear M, Dayan P, Johnstone EC, Meyer-Lindenberg A, Schnyder U, Wang X-J, Bach DR, Fletcher PC. (2016): Charting the landscape of priority problems in psychiatry, part 2: pathogenesis and aetiology. The Lancet Psychiatry 3(1):84-90.

Stephan KE, Friston KJ, Frith CD. (2009a): Dysconnection in Schizophrenia: From Abnormal Synaptic Plasticity to Failures of Self-monitoring. Schizophrenia Bulletin 35(3):509-527.

Stephan KE, Friston KJ, Frith CD. (2009b): Dysconnection in schizophrenia: from abnormal synaptic plasticity to failures of self-monitoring. Schizophr Bull 35(3):509-27.

Stephan KM, Fink GR, Passingham RE, Silbersweig D, Ceballos-Baumann AO, Frith CD, Frackowiak RS. (1995): Functional anatomy of the mental representation of upper extremity movements in healthy subjects. J Neurophysiol 73(1):373-86.

Tibshirani R. (1996): Regression shrinkage and selection via the lasso. Journal of the Royal Statistical Society. Series B (Methodological):267-288.

van den Heuvel MP, Mandl RC, Stam CJ, Kahn RS, Pol HEH. (2010): Aberrant frontal and temporal complex network structure in schizophrenia: a graph theoretical analysis. Journal of Neuroscience 30(47):15915-15926.

Varoquaux G, Gramfort A, Poline J-B, Thirion B. Brain covariance selection: better individual functional connectivity models using population prior; 2010. p 2334-2342.

Vogt BA, Laureys S. (2005): Posterior cingulate, precuneal and retrosplenial cortices: cytology and components of the neural network correlates of consciousness. Prog Brain Res 150:205-17.

Vogt BA, Pandya DN. (1987): Cingulate cortex of the rhesus monkey: II. Cortical afferents. J Comp Neurol 262(2):271-89.

Wang H-T, Guilia P, Charlotte M, Bzdok D, Jefferies E, Smallwood J. (2017): Dimensions of Experience: Exploring the Heterogeneity of the Wandering Mind. Psychological Science.

Weinberger DR, Berman KF, Suddath R, Torrey EF. (1992): Evidence of dysfunction of a prefrontal-limbic network in schizophrenia: a magnetic resonance imaging and regional cerebral blood flow study of discordant monozygotic twins. Am J Psychiatry 149(7):890-7.

Westlye LT, Grydeland H, Walhovd KB, Fjell AM. (2011): Associations between regional cortical thickness and attentional networks as measured by the attention network test. Cerebral cortex 21(2):345-356.

White TP, Joseph V, Francis ST, Liddle PF. (2010): Aberrant salience network (bilateral insula and anterior cingulate cortex) connectivity during information processing in schizophrenia. Schizophrenia research 123(2):105-115.

Whitfield-Gabrieli S, Ford JM. (2012): Default mode network activity and connectivity in psychopathology. Annual review of clinical psychology 8:49-76.

Whitfield-Gabrieli S, Thermenos HW, Milanovic S, Tsuang MT, Faraone SV, McCarley RW, Shenton ME, Green AI, Nieto-Castanon A, LaViolette P. (2009a): Hyperactivity and hyperconnectivity of the default network in schizophrenia and in first-degree relatives of persons with schizophrenia. PNAS 106(4):1279-1284.

Whitfield-Gabrieli S, Thermenos HW, Milanovic S, Tsuang MT, Faraone SV, McCarley RW, Shenton ME, Green AI, Nieto-Castanon A, LaViolette P. (2009b): Hyperactivity and hyperconnectivity of the default network in schizophrenia and in first-degree relatives of persons with schizophrenia. Proceedings of the National Academy of Sciences 106(4):1279-1284.

Woodward ND, Rogers B, Heckers S. (2011): Functional resting-state networks are differentially affected in schizophrenia. Schizophrenia research 130(1):86-93.

Yu Q, Sui J, Kiehl KA, Pearlson G, Calhoun VD. (2013): State-related functional integration and functional segregation brain networks in schizophrenia. Schizophrenia research 150(2):450-458.

Zhou Y, Liang M, Tian L, Wang K, Hao Y, Liu H, Liu Z, Jiang T. (2007): Functional disintegration in paranoid schizophrenia using resting-state fMRI. Schizophrenia research 97(1):194-205.

FIGURES LEGENDS

Figure 1. Target network definitions.

The regions of interest (ROIs) are rendered on the MNI standard brain with frontal, diagonal, and top views. *A* The DMN is represented by 4 ROIs, according to how the main network nodes are frequently studied in neuroimaging research. These comprise the dorsomedial prefrontal cortex (DMPFC), posteromedial cortex (PMC), and right/left temporoparietal junction (TPJ). *B* The DMN nodes are subdivided into 12 ROIs accounting for the distinct subnodes in the DMN that were recently established (Bzdok et al., 2016a; Bzdok et al., 2015; Bzdok et al., 2013; Eickhoff et al., 2016). According to this prior work, the functional core of the DMN ("DMN proper") likely corresponds especially to its blue and red subnodes (the ventral and the dorsal PCCs, the left and right posterior TPJs, and the rostroventral and rostrodorsal DMPFC). *C* The DMN subnodes are supplemented by 9 ROIs for the dorsal attention network (DAN, *light green*) and saliency network (SN, *purple*), drawn from published quantitative meta-analyses (Bzdok et al., 2012; Rottschy et al., 2012). The DAN was composed of the dorsolateral prefrontal cortex (dlPFC) and intra-parietal sulcus (IPS) bilaterally. The SN included the midcingulate cortex (MCC) and the bilateral anterior insula (AI) as well as amygdala (AM). NeuroVault permanent link to all ROIs (21 in total) used in the present study: http://neurovault.org/collections/2216/.

Figure 2. Network analysis workflow.

Exemplary results illustrate the rational of the statistical modeling framework. *A* The *covariance matrix* was computed with brain signals extracted from the DMN atlas. Each entry in this matrix indicates the linear relationship of each specific pair of target DMN nodes. *B* The *precision matrix* was computed by inverse covariance estimation (in this

case without sparsity constraint). In contrast to the covariance matrix, the precision matrix captures the multiple relations between each of the pairs of target nodes while conditioning on the potential influence from the respective other nodes. *C* The *sparse precision matrix* was computed by sparse inverse covariance estimation with sparsity constraint. The additional modeling constraint improves interpretability by automatically reducing the network graph to the important network edges (non-zero strength, *red or blue*) and ignoring the irrelevant ones (zero strength, *white*). *D* The sparse precision matrices were computed separately in healthy controls and schizophrenic patients. Statistically significant group differences in coupling strengths (*brown squares*) were determined by non-parametric hypothesis testing. A significance test assessed group differences between all network relations at once. The entire analysis process was repeated for different network graph definitions (4 versus 12 versus 21 target nodes) and different imaging modalities (resting-state connectivity versus structural morphology).

Figure 3. Studying node versus subnodes in the default mode network.

Significant differences in functional connectivity (*left column*, resting-state functional connectivity [RSFC]) and structural co-occurrence (*right column*, voxel-based morphometry [VBM]). Schizophrenic patients and healthy controls were compared based on the usual DMN nodes (*upper row*) and the topographically more fine-grained DMN subnode atlas (*lower row*). Richer brain signals have been captured by the recent parcellation of the DMN nodes, resulting in a higher number of statistically significant group effects. Analysis approaches based on collapsed DMN nodes may therefore obfuscate disease-specific patterns in fMRI signals as indexed by resting-state

connectivity and in MRI signals as indexed by voxel-based morphometry. The glass brains were created using the nilearn Python package (Abraham et al., 2014).

Figure 4. Dysfunctional connectivity and aberrant structural covariation across networks.

Depicts the significant increase (*red lines*) or decrease (*blue lines*) in functional connectivity (*A*) or in structural co-occurrence (*B*) comparing schizophrenic to healthy subjects in the across-network RSFC analyses (cf. SFig. 1). Circles represent regions of interest in the default mode network (DMN, *orange*), the "DMN proper" (*yellow*), the saliency network (SN, *purple*) and the dorsal attention network (DAN, *light green*). The left column shows the differences within each network, while the right column displays differences between two networks. The connectivity findings show that the dysfunctional connectivities within the DMN include several subnodes that are not part of the "DMN proper". While the functional coupling between the DMN and the SN is partly disrupted, the functional connectivity between the DMN and the DAN is particularly disturbed. Furthermore, the connectivities within and between the SN and the DAN remain largely intact. The covariance findings show that the deviant structural covariations within the DMN involve several subnodes not part of the "DMN proper". The volumetric relationships between the DMN and the SN are also more disrupted than between any other network pair. Collectively, the findings emphasize inter-network dysregulation rather than exclusive disturbance of the DMN core parts. Flat brains were generated using PyCortex (Gao et al., 2015).

Figure 5. DMN aberrations in schizophrenia are specific to subnodes.

Functional connectivity (RSFC) and structural co-occurrence (VBM) measurements were used to compute sparse inverse covariance estimation separately in healthy and schizophrenic individuals (*left column*). We conducted intra-network analyses (i.e., DMN subnode atlas) and across-network analyses (i.e., DMN subnode atlas augmented by nodes of the DAN and SN). Statistically significant group differences (*brown squares* in *middle column*) between the normal and diagnosed individuals are shown in the precision matrix of the schizophrenic group. The number of subnode-specific dysregulations is shown as counts when viewed from the DMN proper (*yellow)*, other DMN parts (*orange),* DAN (*light green),* and SN (*purple*). The findings make apparent that schizophrenia pathophysiology may be relatively more driven by across-network effects and effects outside of the DMN proper. The glass brains were created using the nilearn Python package (Abraham et al., 2014).

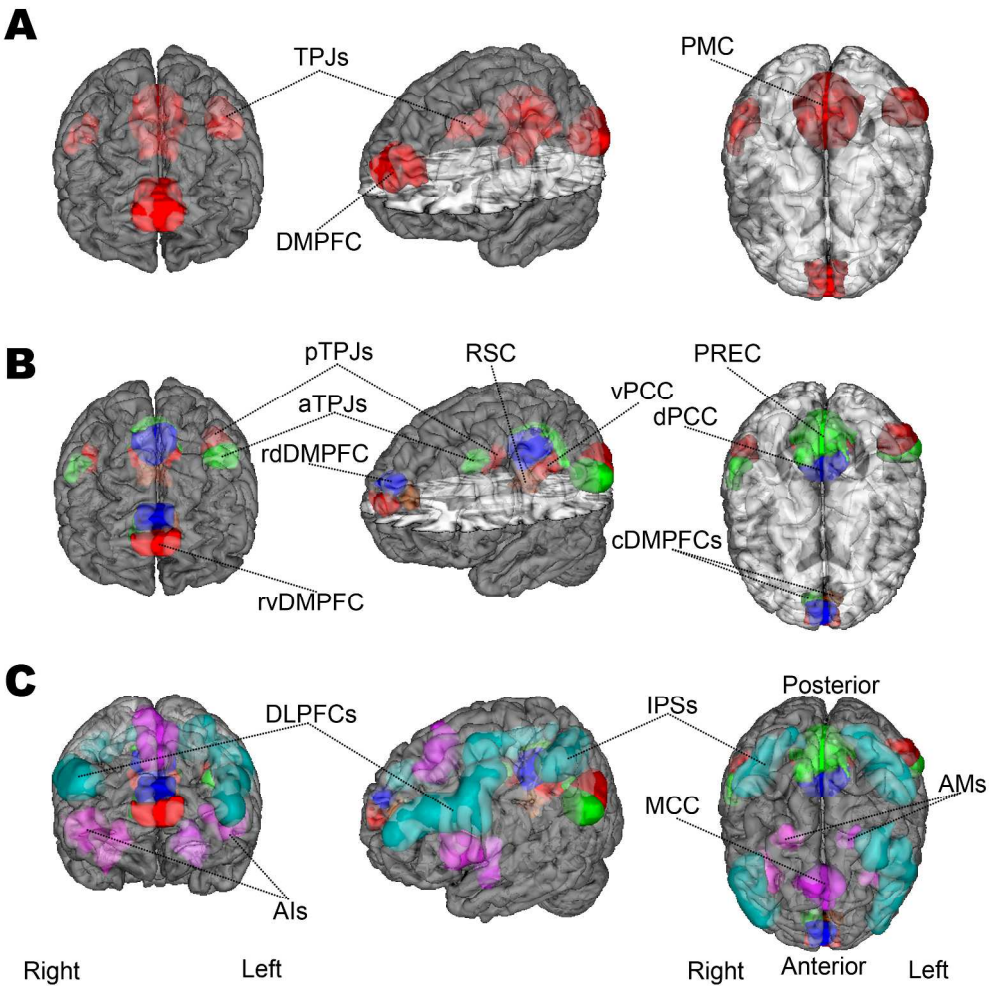

Figure 1. Target network definitions.
The regions of interest (ROIs) are rendered on the MNI standard brain with frontal, diagonal, and top views. A The DMN is represented by 4 ROIs, according to how the main network nodes are frequently studied in neuroimaging research. These comprise the dorsomedial prefrontal cortex (DMPFC), posteromedial cortex (PMC), and right/left temporoparietal junction (TPJ). B The DMN nodes are subdivided into 12 ROIs accounting for the distinct subnodes in the DMN that were recently established (Bzdok et al., 2016a; Bzdok et al., 2015; Bzdok et al., 2013; Eickhoff et al., 2016). According to this prior work, the functional core of the DMN ("DMN proper") likely corresponds especially to its blue and red subnodes (the ventral and the dorsal PCCs, the left and right posterior TPJs, and the rostroventral and rostrodorsal DMPFC). C The DMN subnodes are supplemented by 9 ROIs for the dorsal attention network (DAN, light green) and saliency network (SN, purple), drawn from published quantitative meta- analyses (Bzdok et al., 2012; Rottschy et al., 2012). The DAN was composed of the dorsolateral prefrontal cortex (dlPFC) and intra-parietal sulcus (IPS) bilaterally. The SN included the midcingulate cortex (MCC) and the bilateral anterior insula (AI) as well as amygdala (AM). NeuroVault permanent link to all ROIs (21 in total) used in the present study: http://neurovault.org/collections/2216/.

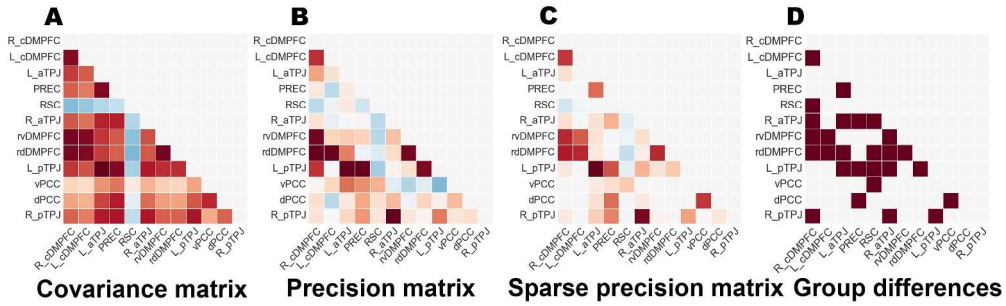

Figure 2. Network analysis workflow.
Exemplary results illustrate the rational of the statistical modeling framework. A The covariance matrix was computed with brain signals extracted from the DMN atlas. Each entry in this matrix indicates the linear relationship of each specific pair of target DMN nodes. B The precision matrix was computed by inverse covariance estimation (in this case without sparsity constraint). In contrast to the covariance matrix, the precision matrix captures the multiple relations between each of the pairs of target nodes while conditioning on the potential influence from the respective other nodes. C The sparse precision matrix was computed by sparse inverse covariance estimation with sparsity constraint. The additional modeling constraint improves interpretability by automatically reducing the network graph to the important network edges (non-zero strength, red or blue) and ignoring the irrelevant ones (zero strength, white). D The sparse precision matrices were computed separately in healthy controls and schizophrenic patients. Statistically significant group differences in coupling strengths (brown squares) were determined by non-parametric hypothesis testing. A significance test assessed group differences between all network relations at once. The entire analysis process was repeated for different network graph definitions (4 versus 12 versus 21 target nodes) and different imaging modalities (resting-state connectivity versus structural morphology).

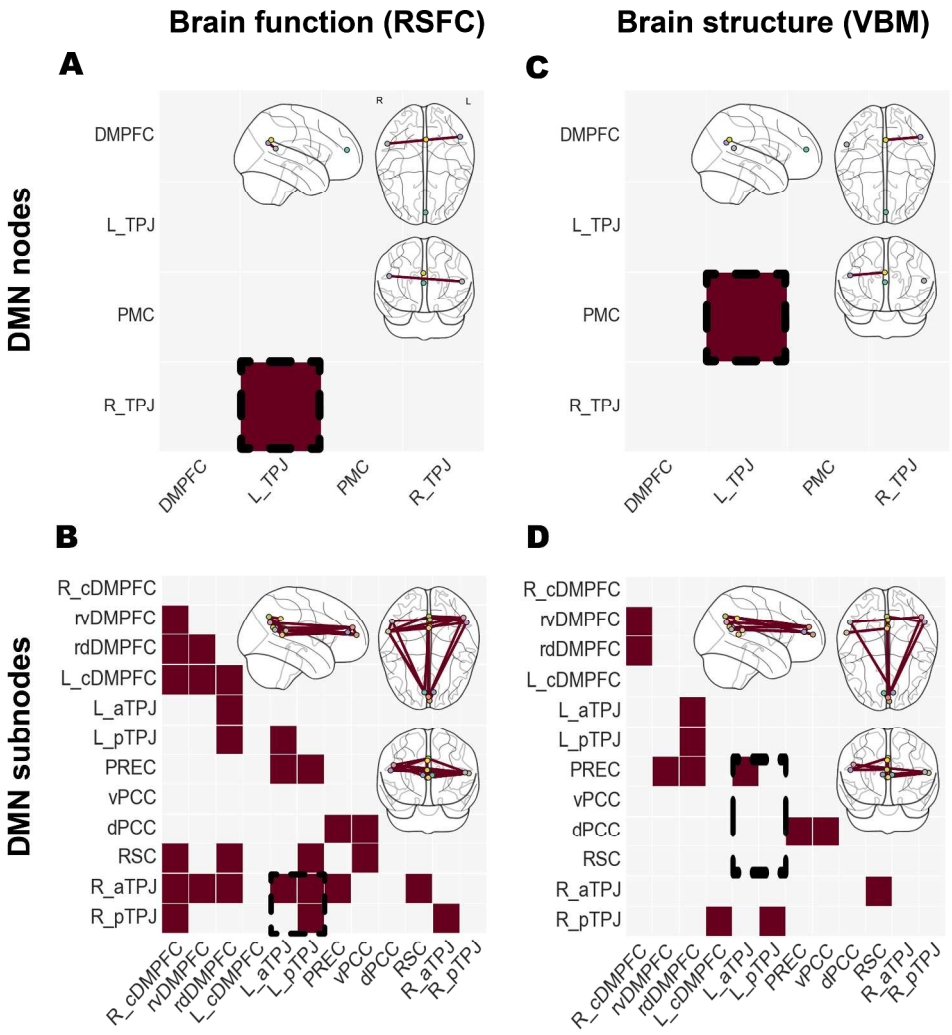

Figure 3. Studying node versus subnodes in the default mode network.
Significant differences in functional connectivity (left column, resting-state functional connectivity [RSFC]) and structural co-occurrence (right column, voxel-based morphometry [VBM]). Schizophrenic patients and healthy controls were compared based on the usual DMN nodes (upper row) and the topographically more fine-grained DMN subnode atlas (lower row). Richer brain signals have been captured by the recent parcellation of the DMN nodes, resulting in a higher number of statistically significant group effects. Analysis approaches based on collapsed DMN nodes may therefore obfuscate disease-specific patterns in fMRI signals as indexed by resting-state connectivity and in MRI signals as indexed by voxel-based morphometry. The glass brains were created using the nilearn Python package (Abraham et al., 2014).

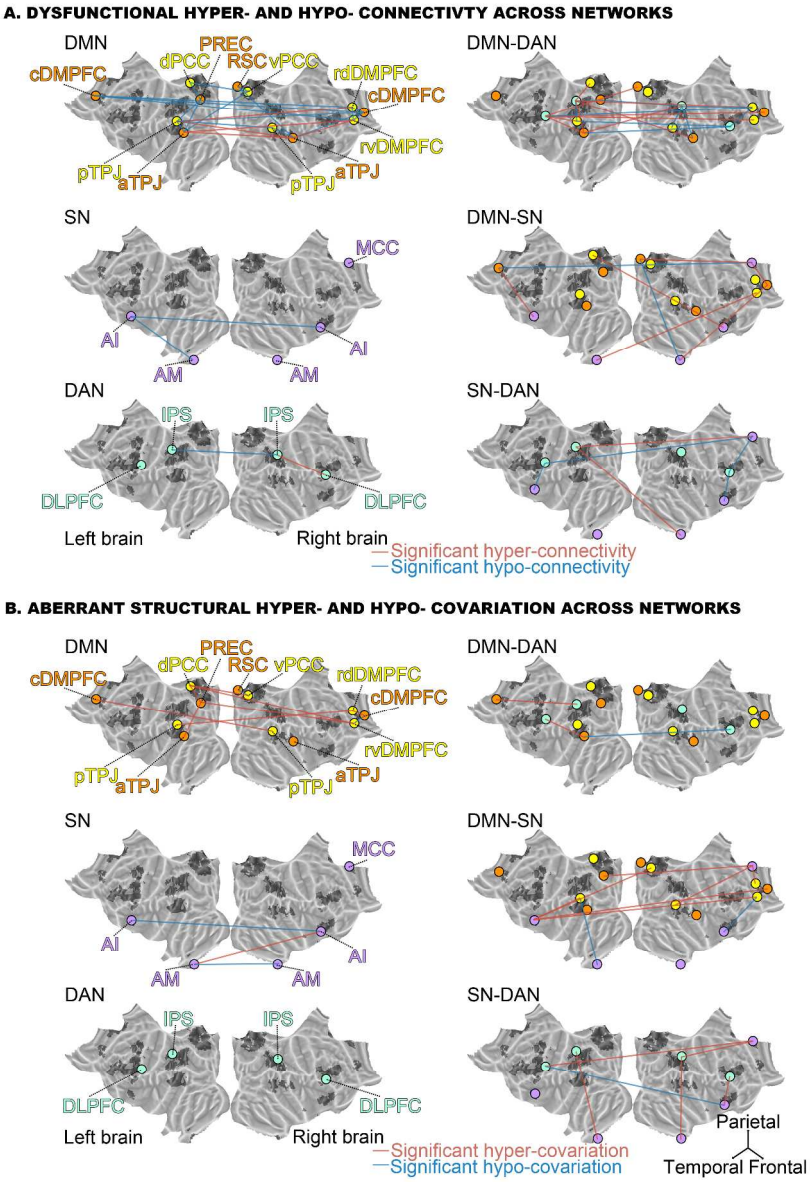

Figure 4. Dysfunctional connectivity and aberrant structural covariation across networks. Depicts the significant increase (red lines) or decrease (blue lines) in functional connectivity (A) or in structural co-occurrence (B) comparing schizophrenic to healthy subjects in the across-network RSFC analyses (cf. SFig. 1). Circles represent regions of interest in the default mode network (DMN, orange), the "DMN proper" (yellow), the saliency network (SN, purple) and the dorsal attention network (DAN, light green). The left column shows the differences within each network, while the right column displays differences between two networks. The connectivity findings show that the dysfunctional connectivities within the DMN include several subnodes that are not part of the "DMN proper". While the functional coupling between the DMN and the SN is partly disrupted, the functional connectivity between the DMN and the DAN is particularly disturbed. Furthermore, the connectivities within and between the SN and the DAN remain largely intact. The covariance findings show that the deviant structural covariations within the DMN involve several subnodes not part of the "DMN proper". The volumetric relationships between the DMN and the SN are also more disrupted than between any other network pair. Collectively, the findings emphasize

inter-network dysregulation rather than exclusive disturbance of the DMN core parts. Flat brains were generated using PyCortex (Gao et al., 2015).

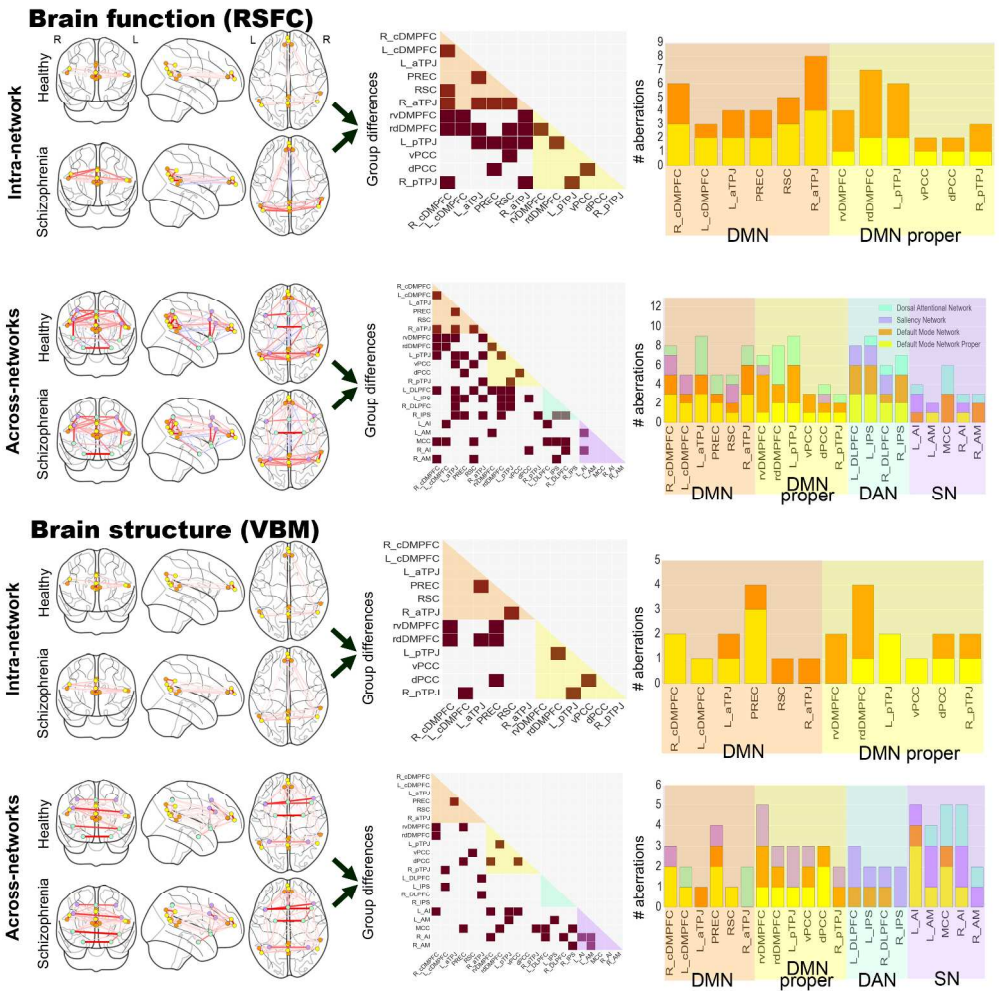

Figure 5. DMN aberrations in schizophrenia are specific to subnodes.
Functional connectivity (RSFC) and structural co-occurrence (VBM) measurements were used to compute sparse inverse covariance estimation separately in healthy and schizophrenic individuals (left column). We conducted intra-network analyses (i.e., DMN subnode atlas) and across-network analyses (i.e., DMN subnode atlas augmented by nodes of the DAN and SN). Statistically significant group differences (brown squares in middle column) between the normal and diagnosed individuals are shown in the precision matrix of the schizophrenic group. The number of subnode-specific dysregulations is shown as counts when viewed from the DMN proper (yellow), other DMN parts (orange), DAN (light green), and SN (purple). The findings make apparent that schizophrenia pathophysiology may be relatively more driven by across-network effects and effects outside of the DMN proper. The glass brains were created using the nilearn Python package (Abraham et al., 2014).